Click Coupling of Flavylium Dyes with Plasmodione Analogues: Towards New Redox-Sensitive Pro-Fluorophores

Baptiste Dupouy, Leandro Cotos, Annika Binder, Lucie Slavikova, Matthias Rottmann, Pascal Mäser, Denis Jacquemin, Markus Ganter, Elisabeth Davioud-Charvet, Mourad Elhabiri

Click Coupling of Flavylium Dyes with Plasmodione Analogues: Towards New Redox-Sensitive Pro-Fluorophores

Baptiste Dupouy,[a] Leandro Cotos,[a] Annika Binder,[b] Lucie Slavikova,[a] Matthias Rottmann,[c] Pascal Mäser,[c,d] Denis Jacquemin,[e,f] Markus Ganter,[b] Elisabeth Davioud-Charvet,[a] and Mourad Elhabiri[a]*

[a] Baptiste Dupouy, Dr Leandro Cotos, Dr Lucie Slavikova, Dr Elisabeth Davioud-Charvet, Dr Mourad Elhabiri
Laboratoire d'Innovation Moléculaire et Applications, UMR 7042, CNRS-Unistra-UHA,
ECPM, 25 Rue Becquerel, 67200 Strasbourg (France)
E-mail: elhabiri@unistra.fr

[b] Annika Binder, Dr Markus Ganter
Heidelberg University, Medical Faculty,
Centre for Infectious Diseases,
Im Neuenheimer Feld 324/344, 69120 Heidelberg (Germany)

[c] Dr Matthias Rottmann, Dr Pascal Mäser
Swiss Tropical and Public Health Institute,
Kreuzstrasse 2, CH-4123 Allschwil (Switzerland)

[d] Dr Pascal Mäser
University of Basel,
Petersgraben 1, CH-4001 Basel (Switzerland)

[e] Pr Denis Jacquemin
Nantes Université, CNRS,
CEISAM, F- 44000 Nantes, (France)

[f] Pr Denis Jacquemin
Institut Universitaire de France (IUF),
F-75005 Paris (France)

Supporting information for this article is given via a link at the end of the document.

Abstract: The development of redox-sensitive molecular fluorescent probes for the detection of redox changes in *Plasmodium falciparum*-parasitized red blood cells remains of interest due to the limitations of current genetically encoded biosensors. This study describes the design, screening and synthesis of new pro-fluorophores based on flavylium azido dyes coupled by CuAAC click chemistry to alkynyl analogues of plasmodione oxide, the key metabolite of the potent redox-active antimalarial plasmodione. The photophysical and electrochemical properties of these probes were evaluated, focusing on their fluorogenic responses. The influence of both the redox status of the quinone and the length of the PEG chain separating the fluorophore from the electrophore on the photophysical properties was investigated. The fluorescence quenching by photoinduced electron transfer is reversible and of high amplitude for probes in oxidized quinone forms and fluorescence is reinstated for reduced hydroquinone forms. Our results demonstrate that shortening the PEG chain has the effect of enhancing the fluorogenic response, likely due to non-covalent interactions between the two chromophores. All these systems were evaluated for their antiparasitic activities and fluorescence imaging suggests the efficacy of the fluorescent flavylium dyes in *P. falciparum*-parasitized red blood cells, paving the way for future parasite imaging studies to monitor cellular redox processes.

Introduction

Involved in a wide range of biological processes and signaling pathways, reactive oxygen and nitrogen species (RONS) or reactive nitrogen species (RNS) are small redox molecules that are produced and tightly regulated by cells.[1] However, increases in their levels can lead to changes in redox homeostasis, resulting in oxidative damage to a variety of biomolecules (nucleic acids, carbohydrates, lipids or proteins), leading to loss of molecular and cellular functions and ultimately to pathological processes (neurological diseases, cancer, diabetes mellitus, cardiovascular diseases or aging, among others).[2] Endogenous enzymatic (e.g. catalase CAT, superoxide dismutase SOD, glutathione peroxidase GPx, thioredoxin) and non-enzymatic (e.g. uric acid, bilirubin, glutathione GSH) antioxidant defense systems closely interact with exogenous compounds (e.g. polyphenols, carotenoids, vitamins, minerals....) to maintain this redox homeostasis. In view of its importance, the development of fluorescent reporters such as small molecule probes for the monitoring of dynamic changes in the redox state[3,4] will facilitate the study of relevant physiological and pathological processes.

This is particularly important, for example, in the development of antiparasitic drug candidates and in understanding their mechanism of action (MoA). Indeed, despite the critical influence of redox environment on key parasitic events (e.g. hemoglobin digestion, heme crystallization, drug partitioning, resistance, and oxidative stress), redox mapping of *Plasmodium falciparum*-parasitized red blood cells (pRBCs) still remains difficult,[5,6] and

small-molecule redox probes are extremely limited.[7] Progress has been made with genetically-encoded redox biosensors derived from green fluorescent protein (GFP), such as, redox-sensitive yellow FP - rxYFP, redox-sensitive GFPs roGFPs, and HyPer.[8-10] These have been successfully employed for measurement of the glutathione redox potential in the parasite cytosol[9,11,12] but are, however, not suited for redox measurements under acidic conditions.[13] Such genetically-encoded probes for redox mapping of *P. falciparum* parasites are furthermore difficult to handle due to the time and resources needed for their construction, and display limitations, e.g. blue/green/yellow fluorescence; red FPs mainly based on sea organisms;[14] no two-photons absorption (TPA) properties excepted for proteins with λ_{em} > 600 nm; and no post-functionalization possible. The search for novel small-molecule probes for *in situ* real-time monitoring thus remains of paramount importance to get further insight into the MoA of current and ongoing antimalarial drugs and for producing reliable data with regard to candidate parameters contributing to drug resistance.

The low and transient physiological concentrations of most RONS (reactive oxygen and nitrogen species)[15,16] indeed require selective, rapid, and reversible detection strategies, with the development of bright fluorophores allowing detection across a broad spectrum of wavelengths (visible-red-NIR). Such fluorophores should also benefit from substantial Stokes shifts and possess tuneable electrochemical properties to span the whole range of biologically relevant redox potentials. In addition to these constraints, good solubility in water, biological compatibility (i.e., membrane permeability, subcellular localization, no cytotoxicity, no alteration of the cellular redox homeostasis, low protein interference), specificity for the target organelle are several essential parameters to be considered.[17]

Many fluorescent systems have been described for the detection of redox processes,[15,18-21] but they are very often based on irreversible or reaction-based interactions between RONS and the probe, thus precluding accurate assessments of redox changes and intracellular fluctuations (e.g. chronic high or transient levels of RONS).[3,22,23] Reversible probes[24] overcome this limitation and allow the monitoring of temporal changes in the redox state of living cells. Several reviews[25-27] provide a complete overview of the reversible[28] redox probes available to date. The strategy commonly used to obtain such fluorescent redox probes consists of using electrophores (e.g. molecular scaffolds or metal complexes, Scheme 1),[29] whose response to an (electro)chemical stimulus is reversible (e.g. nitroxyl radicals,[19] quinone/hydroquinone,[30] chalcogen-based derivatives with sulphur, selenium or tellurium,[19,31] flavins, tetrathiafulvalenes…) and whose redox state can alter the fluorescence of a covalently linked fluorescent unit, typically through Photoinduced electron Transfer (PeT).

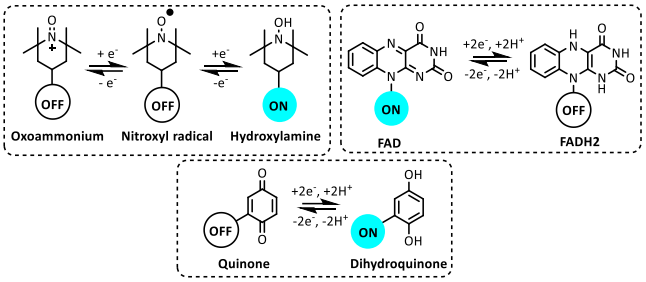

Scheme 1. Reversible redox-sensitive units commonly reported and used to construct redox-responsive fluorescent probes for biological applications.

Other redox-responsive systems with intrinsic adjustable fluorescence properties (ON-OFF or ratiometric systems) depending on their oxidation state and allowing a reversible reaction can also be mentioned, e.g. blue-emitting resazurin/pink-emitting resorufin/non fluorescent dihydroresorufin,[32] blue-emitting dihydroethidine/red-emitting ethidium,[33] red-NIR-emitting methylene blue/non fluorescent leucomethylene.[34]

With particular reference to fluorescent redox probes based on hydroquinone/quinone pair, Scheme 2 provides an overview of the photophysical properties, photoinduced mechanism and efficiency of different systems described so far. Most of the systems described are based on quinones conjugated or fused to fluorescent dyes such as Ru(bipy), bodipy, rhodamine, triazine or cyanine complexes. Quinones coupled to fluorophores via a spacer are less common examples and no approach has been described to evaluate the effect of the length of the spacer (e.g. PolyEthylene Glycol PEG-type). For example, the red luminescent compounds $[Ru(bipy)_2(bipy\text{-}Q)]^{2+}$[35] and $[Ru(bpy)^2(PAIDH)]^{2+}$[36], based on a Ru(II) center, yield a 4-fold (luminescence spectra of the isolated compounds) and 600-fold (luminescence spectra obtained by exhaustive electrolysis) increase, respectively, after reduction of the quinone moiety. However, these systems are characterized by low quantum yields in degassed solution and have not been applied to biological systems. Redox-responsive fluorescent probes were also designed using a bodipy reporting scaffold as exemplified by BD-PHQ[37] (110-fold increase upon reduction with 1.1 M sodium ascorbate in 5% v/v Triton–X/H_2O) or H2B-QH2[38] (200-fold increase upon reduction with $NaBH_4$). None of these two models was applied in a biological system. Of interest is a related aza-bodipy[39] coupled to an *ortho*-quinone whose redox-response was achieved by pH variation (oxidation under basic conditions and reversible reduction at acidic pH). Hydroquinones are indeed known to undergo autoxidation under basic conditions.[40] This aza-bodipy was successfully used to monitor extracellular pH difference between normal tissue and tumour both *in vitro* U87 glioma and *in vivo* breast cancer in mice. Also worth mentioning is the reversible photoacoustic probe, BDP-DOH, based on a bodipy reporter and a quinone sensor, which has been used to image the local redox state *in vivo* by monitoring dynamic changes in the redox couple, superoxide anion ($O_2^{\bullet-}$) and GSH.[41] Also, in the bodipy field, the engineered compound FerriBRIGHT[42] is one of rare compounds (with TCAO and PY-CAO, *vide infra*) in which the oxidized quinone form is fluorescent

while the reduced hydroquinone state undergoes a PeT quenching. When combined with a cyanine fluorophore, the dopamine-based DA-Cy[43] compound undergoes a 20-fold decrease in fluorescence during oxidation, a process that is irreversibly reversed by the addition of thiols. This system was implemented in living HL-7702 cells and fresh rat hippocampus tissues to image H_2O_2 oxidation and thiols reduction processes. Similarly, a related water-soluble cyanine dye[40] has been described as able to reversibly respond to oxidation ($NaIO_4$) or reduction (GSH, 16-fold increase) reactions. In particular, for bioreductants such as GSH, cysteine or ascorbate, the emission centred at 660 nm was restored in short times (~ 30 s). This system has been applied to image living cells (A549 and J774.1). As additional examples, the 1,4-benzoquinone/rhodamine-based probe (Rh-Q)[44] and its related analogues also act as fluorogenic probes and were shown to undergo a 6-fold fluorescence quenching upon oxidation with excess of $[Cu(phen)_2]^{2+}$, which can be rapidly reversed by the addition of cysteine. This probe was readily internalized by HeLa living cells and predominates in the form of hydroquinone due to the reducing milieu. However, these probes were difficult to be oxidized *in vitro* either by $[Cu(phen)_2]^{2+}$ or after permeabilization with saponine followed by addition of H_2O_2 and horseradish peroxidase. Of interest is also the quinone-triazine (TCA) probe that can respond to one (1P) or two-photon (2P) excitation. Oxidation by $O_2^{\bullet-}$ generates TCAO that displays 1000- and 3-fold greater fluorescence emission upon 1P and 2P excitation, respectively. TCAO was reversibly reduced to TCA by GSH[45] and this dye was successfully used in dual-mode fluorescence imaging for tracking $O_2^{\bullet-}$ fluctuations in hepatocytes, zebrafish and mice during mimicked ischemia-reperfusion injury. Similar to TCAO, the 1P and 2P PY-CA[46] fluorogenic probe is also oxidatively turned on with $O_2^{\bullet-}$ (1000-fold greater fluorescence emission upon 1P excitation) and quenched by GSH. The oxidized PY-CAO has been used for imaging of $O_2^{\bullet-}$ levels in 4T1 cells, in a mouse tumour tissue and in wild-type *Caenorhabditis elegans* worms. Finally, to complete this non-exhaustive survey, naphtho[2,3-c]pyran-5,10-dione was used for developing fluorescent redox probes.[47] While the oxidized form is not fluorescent, reduction with $NaBH_4$ afforded a red fluorescent (Φ = 0.07) hydroquinone when substituted with *N,N*-dimethylaminophenyl. A highly reversible ON/OFF push-pull system was developed by combining a fluorescent dansyl moiety with a phenyl-carbazoloquinone redox sensor via an NH bridge.[48] Neither of these last two examples has been used in a biological investigation.

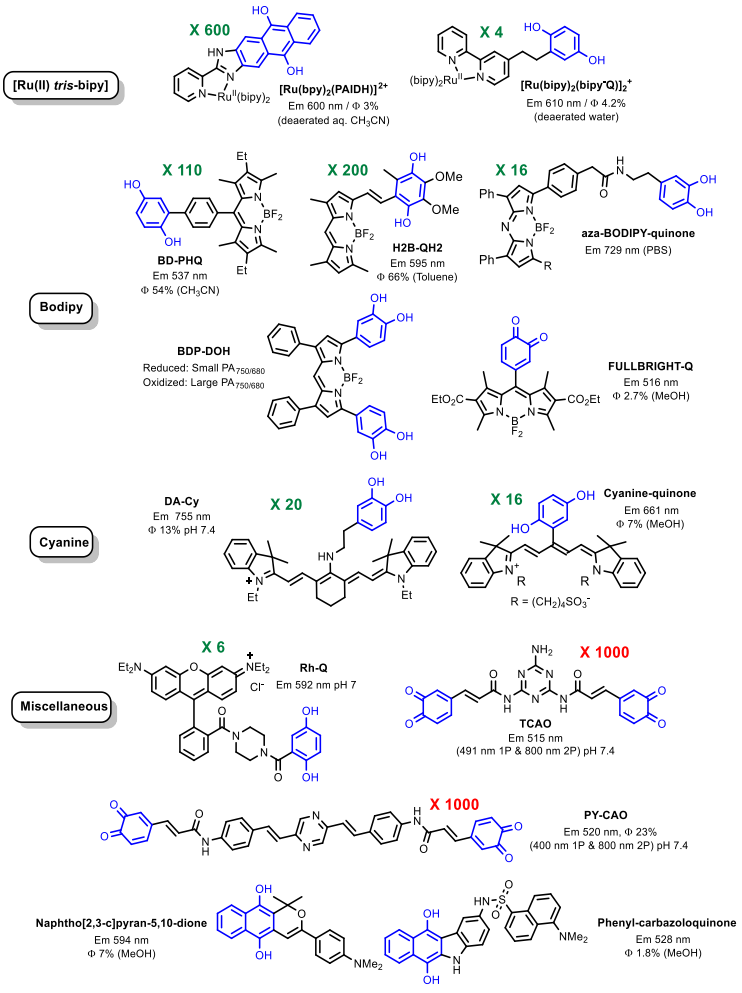

Scheme 2. Chemical structures and photophysical properties of fluorescent redox probes based on hydroquinone/quinone pair (red: increased fluorescence upon oxidation; green: increased fluorescence upon reduction).

Our team has recently developed lab-made fluorescent tools derived from flavylium ions whose properties and chemical structure can be tailored to the desired applications.[49] Using straightforward synthetic routes, bright, water-soluble, stable (aqueous stability of these compounds up to pH > 9)[49] and photostable azide dyes were accessible at the 100 mg scale thus allowing the preparation, characterization and investigation of the click adducts with alkynyl-3-benzoylmenadiones (benzoyl-MD alkyne), a series of redox-active derivatives recently developed as photoaffinity labelling agents – upon (photo)reduction – for activity-based protein profiling ABPP.[50,51] Of note, the parent 3-benzylmenadiones, represented by the lead compound called plasmodione (**PD**), display potent antimalarial activities.

Following a preliminary study, we observed that the adducts clicked with the benzoyl-MD alkynes were almost fully quenched compared to the flavylium PEG-azide fluorophore (Scheme 3) likely due to a PeT process, while under their protected state (i.e. 1,4-dimethoxy-naphthalene core), no fluorescence quenching was observed. Following this observation, we thus postulated that the reduced species might display the same redox properties as the protected benzoyl-MD, allowing an OFF-ON fluorogenic property in response to an enzymatic reduction. In this work, we report on the design and selection of fluorescent probes and click adducts, their synthesis, detailed photophysical and electrochemical characterization, and antiparasitic activities. The influence of the length of the PEG chain on the fluorogenic response was also investigated. Finally, fluorescence of flavylium dyes was visualized in living pRBCs to demonstrate their effective penetration, paving the way for future imaging approaches to measure redox processes within pRBCs.

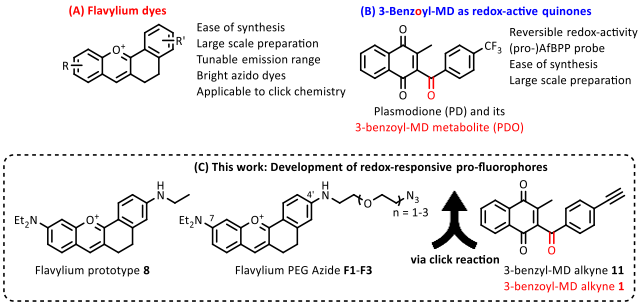

Scheme 3. Chemical structures of the tools investigated in this work and main objectives.

Results and Discussion

Screening and Selection Approach

In our previous study,[49] we developed azide fluorophores based on rigid flavylium dyes connected to a terminal azide function separated by a variable-length PEG chain. We were able to reach bright compounds (**F1**-**F3**, Scheme 3) emitting in the red/far red domain and demonstrated that the length of the PEG chain (1 to 3 monomers) had no influence on the photophysical properties of the dye. Interestingly, the Copper(I)-catalyzed Alkyne-Azide Cycloaddition (CuAAC) cycloaddition of a benzoyl-MD with one of those containing a PEG-2 chain showed a strong quenching of the fluorescence emission of the dye (*vide infra*) suggesting that photoinduced processes occurred within the hybrid molecule. To deepen our understanding, we carried out a simple screening by absorption/emission plate reading with the PEG-2 analogue to pinpoint the best substitution pattern for achieving both the highest brightness and the largest response amplitudes upon click reaction with the benzoyl-MD alkyne (**1**) (described in reference[50,51] under the same compound code). Since the fluorophore can be generated in a final step by condensation in an acidic medium (EtOH/H_2SO_4), the previously described tetralone-PEG-2-azide (**2**)[46] intermediate was first subjected to a CuAAC-type cycloaddition reaction with benz(o)yl-MD alkyne (**1**) and (**11**) and reduced analogue protected as a 1,4-dimethoxy-naphthalene (**10**) (described in references 50 and 51 under the same compound code) (Scheme 4). A first screening carried out with 15 different salicylaldehydes allowed comparing the flavylium-PEG-2-azide dye **F2** with their derivative clicked to **1**, and thus assessing the impact of the incorporation of a benzoyl-MD alkyne by CuAAC on the fluorescence emission properties of the dye (Figures S1-S16 in the ESI). Optical measurements and comparisons between the different systems can be indeed made without the need for purification, as the visible absorption and fluorescence signal is generated by the newly formed flavylium moiety. The emission spectra were normalized to the absorbance at the excitation wavelength to allow direct comparison of all dyes generated in the wells (Scheme 4).

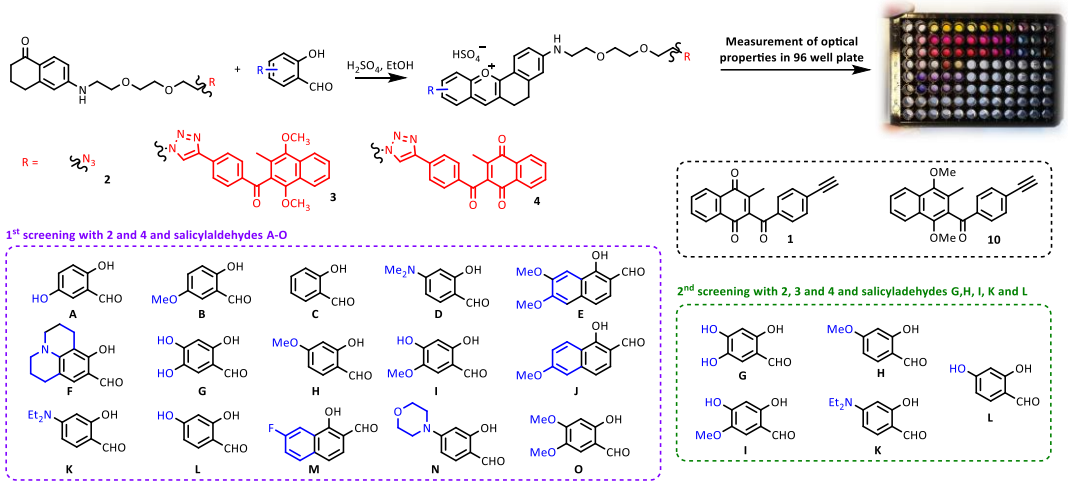

Scheme 4. Screening (by absorption and emission) of PEG-2 dyes by varying the substitution of the dye using 15 salicylaldehyde derivatives and the substitution of the PEG using **2**, **3** and **4**.

Comparison of the spectroscopic data (Table 1) provided valuable information. The incorporation of a benzoyl-MD unit by click chemistry always leads to a quenching of the fluorescence emission (at least half the emission of flavylium PEG azide). Flavylium dyes with alkylamino (**2-D**, **2-K** and **2-N**) or dimethoxy (**2-O**) substitutions, which act as electron donor groups (EDG), showed the strongest quenching effects. The same dyes, among some others (**2-D**, **2-G**, **2-I**, **2-K, 2-N** and **2-O**, Table 1), are also the brightest compounds in their free azido form. The incorporation of a benzoyl-MD moiety (**4**) by click chemistry therefore results in a significant extinction of the emission intensity of the dye but does not alter markedly its position or shape, suggesting the absence of direct interactions in the excited state between the two chromophores (i.e. the flavylium and benzoyl-MD core). Similarly, no significant change in the absorption spectra was observed hinting that there is no precipitation or π-π stacking. Last, extending the π-electron delocalization with an additional phenyl ring (salicylaldehydes **2-E**, **2-J** and **2-M**) does not specifically modify the emission wavelength of the flavylium ion and results in dyes of lowest brightness (Table 1).

Table 1. Photophysical data[a] recorded for the flavylium dyes generated in the wells by reaction of **2**, **3** and **4** with salicylaldehydes **A-O** in ethanol with excess of sulfuric acid.

	Dyes (w/**2**)			Dyes (w/**4**)	Dyes (w/**3**)
Sal.	λ_{abs}	λ_{em}	FI	FI *vs* dyes (w/**2**)	FI *vs* dyes (w/**2**)
A	531/557sh	598/646	6.6	x 0.48	
B	530/557sh	596/646	7.8	x 0.45	
C	518	587/633/689	5.3	x 0.48	
D	583	635	**28.1**	x 0.13	
E	555/578sh	615/669	5.6	x 0.43	
F	579/615sh	654	10.3	x 0.31	
G	561	604/649	**26.1**	x 0.36	x 1.22
H	535sh/554	594/636	14.2	x 0.5	x 1.79
I	560	603/647	**23.2**	x 0.34	x 1.01
J	580/554sh	619/670	5.6	x 0.45	
K	605	638	**71.7**	**x 0.20**	**x 1.04**
L	535sh/556	595/636	11.1	x 0.37	x 1.53
M	543	613/663	2.6	x 0.56	
N	587	635	**35.0**	**x 0.20**	
O	560	605/649	**20.6**	**x 0.25**	

[a] λ_{abs} and λ_{em} in nm, FI = Fluorescence Intensity in 10^2 ua. Sal = salicylaldehyde. w/ = with.

A second screening experiment using the same approach was performed using only five selected salicylaldehydes (**G**, **H**, **I**, **K** and **L**) with tetralones **2** and **3** (Scheme 4 and Figures S17-S21 in the ESI). Compound **3** was obtained by CuAAC reaction between **2** and **10**, which is the reduced form of **1** protected by methyl group to prevent the spontaneous oxidation of the dihydroquinone into the quinone moiety (see ESI). This chemical modification results in benzoyl-MDs that are much less oxidizing (*vide infra*) and more electron-rich. Interestingly, no fluorescence quenching was observed when **3** (Table 1) was used demonstrating that the electronic poorness (oxidized benzoyl-MD, **1**) or richness (reduced benzoyl-MD, **10**) of the naphthoquinone is critical for quenching the emission of the combined fluorophore. These results thus suggest that PeT can take place between the flavylium dye, acting as an electron donor, and the benzoyl-MD in its oxidized form, an electron acceptor. Upon reduction, the electron quinone acceptor becomes less oxidizing, as only the ketone of the benzoyl moiety can be reduced (*vide infra*). This renders the PeT process thermodynamically not favoured and thus does not alter the fluorophore emission. Absorption and emission measurements confirmed that the dye derived from salicylaldehyde **K** was the best compromise, with high brightness and quenching amplitude in the presence of the oxidized benzoyl-MD.

Synthesis

We synthesized the hybrid molecules using salicylaldehyde **K** and the alkynes derived from oxidized benzoyl-MD **1** and the reduced/protected benzoyl-MD **10**. Furthermore, we investigated how the length of the PEG spacer linking the flavylium to the

redox-active moiety (the benzoyl-MD) affects the optical properties of the click adducts. Three PEG spacer lengths were selected: short (n = 1), intermediate (n = 2) and long (n = 3). Following the screening approach (*vide supra*), we were able to assess the best decoration for the optimized optical properties of the flavylium fluorophore using salicylaldehyde **K**. The syntheses of flavylium azide dyes containing a short (**F1**, n = 1) or intermediate (**F2**, n = 2) PEG chain[49] and of compounds **1** and **10**[51] have been described previously. Two synthesis strategies have been implemented.

First, **F1** was clicked with **10** and **1** in acetonitrile in the presence of $Cu(CH_3CN)_4(BF_4)$ and bathocuproin to afford compounds **F1-10** and **F1-1**, respectively, in good yields (Scheme 5). Following this approach, **F2-1** containing a PEG-2 chain was prepared from **F2** and **1** using the same experimental conditions. Alternatively, we have also demonstrated that **F2-1** can be synthesized by first a CuAAC reaction of the α-tetralone functionalized in position 6 by a PEG-2-azide moiety (**2**) with the benzoyl-MD alkyne **1** to give the click α-tetralone **4** in excellent yields (97%). Acid condensation (HCl gas generated *in situ* by reaction of acetyl chloride with ethanol in ethyl acetate) of **4** with salicylaldehyde **K** then afforded **F2-1** in a global 69% yield for the two steps. The same strategy was used to obtain the homologous dye **F2-10** in a two-step process with a total ~ 50 % yield. These two approaches demonstrate the versatility of our synthetic strategy, as the CuAAC reaction can be carried out as either the first or the second step in the proposed synthetic routes. The dyes with the longest PEG chain (n = 3) were obtained from the α-tetralone PEG-3-azide **5** by CuAAC click reaction with the alkynes **10** and **1** followed by acid condensation. These two steps were carried out without purification of the intermediates **6** and **7** to afford the final compounds **F3-10** and **F3-1** in moderate overall yields of 30-40%.

Photophysical Properties

A simple screening strategy based on a simple chemical reaction (condensation of a α-tetralone and a salicylaldehyde under acidic conditions) was implemented to generate a library of spectroscopic data (absorption and emission) for almost 40 different combinations. This approach has provided essential information and allowed synthesis efforts to be focused only on the most promising derivatives (Scheme 5). A photophysical characterization of the flavylium-PEG-azides has already been carried out in a previous work[49] and has shown high brightness (quantum yields in the range of 25-30%) for the red/far red emitting systems, without any significant influence of the length of the spacer. One of the advantages of using these clickable flavylium-PEG-azides is their solubility in water due to the cationic nature of the dye and the presence of PEG moieties.

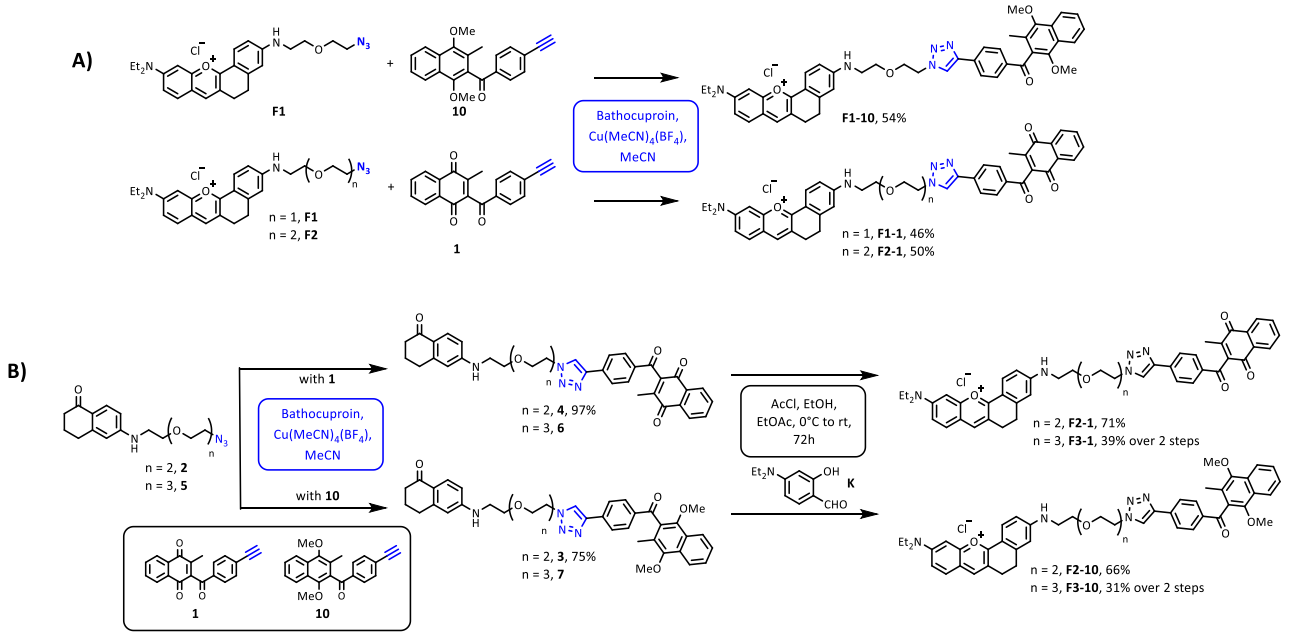

Scheme 5. Synthetic routes (**A**) (acidic condensation – CuAAC) and (**B**) (CuAAC - acidic condensation) for the formation of the click adducts with PEG (n = 1, 2 and 3) chains with **1** or **10**.

Table 2. Photophysical data[a] obtained for the flavylium-PEG-azides and their click adducts with **10** and **1** in buffered aqueous solutions at pH 7.41 containing 0.1 M NaCl.[b,c]

Cpd.	λ_{abs}[a] / λ_{em}[a]	ε[a]	Φ[a]	Stokes shift[a]	B[a]	Exp.
8	594 / 633	3.49	23.0	1040	8.0	[b],[46]
8	599 / 638	5.26	28.3	1020	14.8	[c]
F1	593 / 633	4.55	23.6	1070	10.4	[b],[46]
F1	598 / 638	5.62	26.3	1050	14.8	[c]
F1-1	601 / 633	2.28	1.3	840	0.3	[c]
F1-10	608 / 639	3.71	23.1	800	8.6	[c]
F2	594 / 636	1.76	22.4	1110	3.9	[b],[46]
F2	598 / 638	1.89	30.4	1050	5.7	[c]
F2-1	605 / 640	4.37	2.2	900	1.0	[c]
F2-10	603 / 639	4.32	30.1	935	13.0	[c]
F3	594 / 634	7.49	26.5	1110	19.9	[b],[46]

F3	598 / 637	8.62	27.4	1020	2.36	[c]
F3-1	604 / 637	3.63	6.7	860	2.4	[c]
F3-10	602 / 639	4.64	29.4	960	13.6	[c]

[a] λ_{abs} and λ_{em} in nm, ε in 10^4 $M^{-1}.cm^{-1}$, absolute quantum yield Φ in %, Stokes shift in cm^{-1}, Brightness B in 10^4 M cm^{-1}. [b] Aqueous buffer at pH 7.41 (0.1 M NaCl); [c] Aqueous buffer at pH 7.41 (0.1 M NaCl) containing 15% of DMSO by volume. The errors on the quantum yields Φ, the λ_{abs} and λ_{em} are estimated to be ± 10% and ± 1 nm, respectively. Ref. = reference dye **8** lacking PEG and azide unit (Scheme 3). Additional photophysical data in 100% ethanol are available in Table S2 in the ESI.

However, the synthesized click adducts with the hydrophobic benzoyl-MD **10** or **1** (Scheme 5) showed a significant loss of aqueous solubility (Figure S22 in the ESI). To assess the effect of the presence of the benzoyl-MD (oxidized or reduced/protected states) on the photophysical properties under the best possible conditions, we showed that 15% by volume of DMSO was at least required to reach an appropriate solubility of the click adducts in aqueous buffer (pH 7.41 + 0.1 M NaCl) (Figure S23 in the ESI for **F1-10**). The photophysical data are given in Table 2 and the corresponding absorption, emission and excitation spectra are available in Figures S24-S32 in the ESI.

As already demonstrated,[49] the photophysical data recorded for flavylium-PEG-azides in a water/DMSO (85/15 *v/v*) mixture buffered to pH 7.41 first show that the length of the PEG chain or the addition of DMSO has no significant effect on the emission properties of the fluorophore. These compounds are all characterized by a very bright emission in the red/far red spectral window. Addition by CuAAC of a benzoyl-MD unit in its oxidized form significantly quenches the emission centred on the flavylium dye, confirming the observations deduced from the screening approach. Reduction of the benzoyl-MD electrophore (in its protected form) did not alter the dye emission, demonstrating that its high electron richness prevented the PeT process. A comparison of the quantum yields of adducts with benzoyl-MD in oxidized and reduced forms shows that the shorter the spacer length, the greater the quenching efficiency. For the system based on the shorter PEG chain (n = 1, **F1-1** *vs.* **F1-10**) a quenching efficiency of almost 95% was measured, whereas for the analogue with a longer PEG chain (n = 3, **F3-1** *vs.* **F3-10**) it was only 75% (Figure 1 and Figure S33 in the ESI). Since this process is intramolecular in our case, this significant quenching is most likely explained by the close distance between the electron donor and electron acceptor, which favours the PeT process and results in an efficient fluorogenic system. It has indeed been shown by absorption or emission that no PeT quenching occurs when the prototype dye **8** is combined with the benzoyl-MD **1** (Figures S34 in the ESI). Other intramolecular non-covalent interactions can be also proposed (*vide infra*).

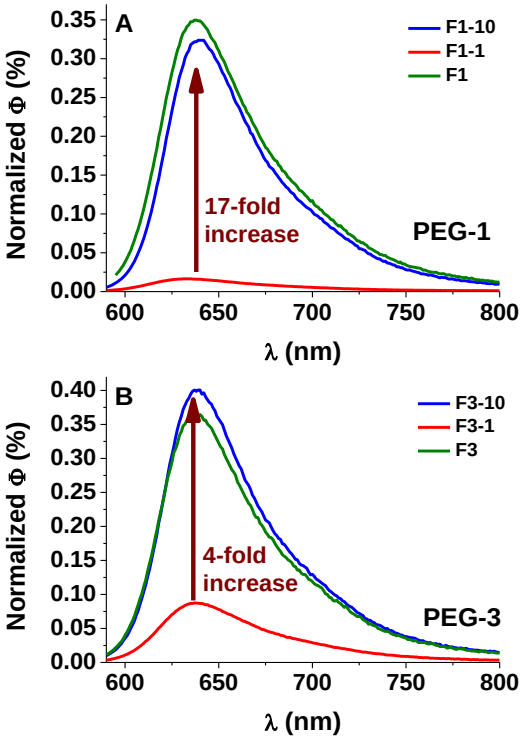

Figure 1. Emission spectra of (A) the flavylium-PEG-1 azide **F1** compared to its click analogues with oxidized (**F1-1**) and reduced/protected (**F1-10**) benzoyl-MDs and (B) the flavylium-PEG-3 azide **F3** compared to its click analogues with oxidized (**F3-1**) and reduced/protected (**F3-10**) benzoyl-MDs recorded in buffered aqueous solution at pH 7.41 (0.1 M NaCl; 15% volume of DMSO). The emission spectra have been normalized with respect to their quantum yield (area under the curve).

DFT Calculations

To ascertain the possibility of PeT with the oxidized benzoyl-MD electrophore,[3] we have performed DFT calculations (see the ESI for details), and the key results are displayed in Figure 3, where we represent the two moieties. The linker being rather long, only through-space transfer can be considered. As the linker is flexible, one can envisage several conformers, but this does not modify the ordering of the key MOs (Figures S62-S63 in the ESI). We have therefore considered the fluorophore and the donor naphthoquinone in both its reduced and oxidized forms. As can be seen, the HOMO of the fluorophore is unsurprisingly the highest, so that after photoexcitation electron transfer from the donor's HOMO cannot take place, a statement holding for both the oxidized and reduced forms. However, the LUMO of the dye is significantly above the one of the quinoidal form, allowing PeT (and hence emission quenching) as shown in Figure 3. In the dihydronaphthoquinone structure, such PeT becomes impossible since the LUMO of the donor becomes too high. These results are consistent with experimental observations. Note that we have also considered the di-OMe-donor and the alignment of the molecular orbitals is mostly unchanged as compared to the di-OH structure.

Redox-Sensitive Fluorescence Properties

Upon reduction and protection as a 1,4-dimethoxy-naphthalene core, the electron richness of the naphthoquinone increases making it unresponsive to reduction (*vide supra*). In that case, PeT is prevented, leading to fluorophores as bright as the parent flavylium-PEG azides **F1**-**F3**. As mentioned above, **PDO**$_{ox}$ can be reduced to **PDO**$_{red}$ in a continuous redox cycle in pRBCs.

Following this concept, we thus postulate that the hybrid molecules, similarly to **PDO**$_{ox/red}$, can display the same redox behaviour, allowing an OFF-ON fluorogenic property in response to enzymatic reduction (*vide infra*).

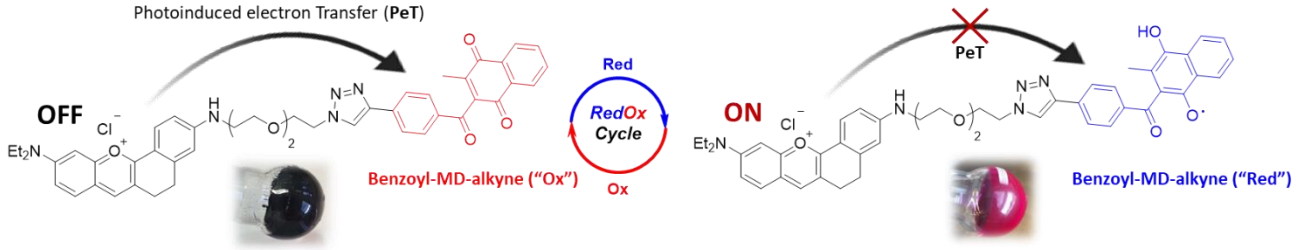

Figure 2. Schematic representation of the influence of the redox state (only the 1-electron reduced species is represented here) of the benzoyl-MD unit on the emission properties of the flavylium dye. Images of the isolated products **F2-1** and **F2-10** have been used in this figure to illustrate this mechanism.

To provide an experimental proof of concept, **F2-1** was reduced by photoirradiation at 365 nm. UV-photoreduction of (benzo)quinones in propan-2-ol (*i*PrOH) is known to generate semiquinone radicals and dihydroquinone.[52-54] Upon UV-excitation, the photo-excited 1,4-naphthoquinone core generates an triplet state that can be trapped by an hydrogen atom donor such as *i*PrOH.[55,56] Photoirradiation at 365 nm[54] in *i*PrOH for 90 minutes of **F2-1** resulted in a strong enhancement (4-fold increase) of the fluorescence emission (Figure 4) compared to a non-illuminated sample. This clearly substantiates that the reduction of the benzoyl-MD moiety prevents the PeT quenching and reinstates partly the fluorescence emission of the flavylium dye. It should also be noted that the absorption spectra of the irradiated and non-irradiated solutions were only slightly affected (decrease of less than 12% in the main absorption), demonstrating the high photostability of the flavylium fluorophore when subjected to a strong and continuous UV photoexcitation for a very long period (90 minutes).

We also tested the reduction of **F2-1** by reaction with 1 mM solution of bio-reductants such as GSH and cysteine (Cys) for 24 hours. An increase in fluorescence was also observed, but less than under photoirradiation (2.4-fold for GSH and 2.7-fold for Cys). In addition, a significant decrease in the main absorption band was observed, demonstrating a loss of fluorophore stability under these experimental conditions (1 mM of GSH or Cys) after 24 hours of reaction (Figures S35 and S36 in the ESI). Although the increase in fluorescence emission does not reach the expected value, the results show that the reduction of **F2-1** is possible in biological media and can be monitored by emission fluorescence.

Redox Properties

Several model compounds were first investigated, including **1** (benzoyl-MD alkyne),[51] **10** (reduced benzoyl-MD alkyne protected by methyl groups) and the flavylium **8** fluorophore prototype (Scheme 3). The analogues with PEG-azide chains were not considered in this study due to the likely electrochemical reduction of the azide function. In DMSO, **1** is characterized by the presence of two waves (1-electron transfer each) separated by about 700 mV (Figure S37 in the ESI).

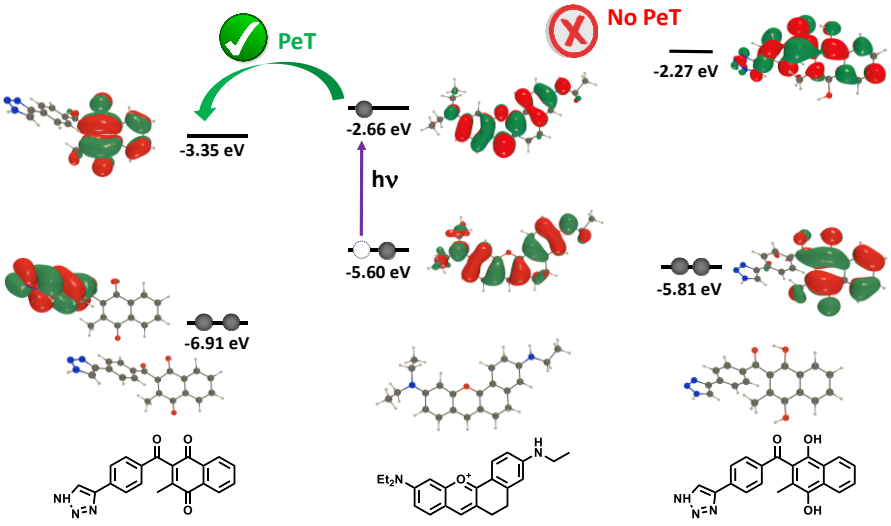

Figure 3. Representation of the frontier MO (energy and topology) of the dye and the oxidized and reduced forms as determined by DFT (see the ESI for details).

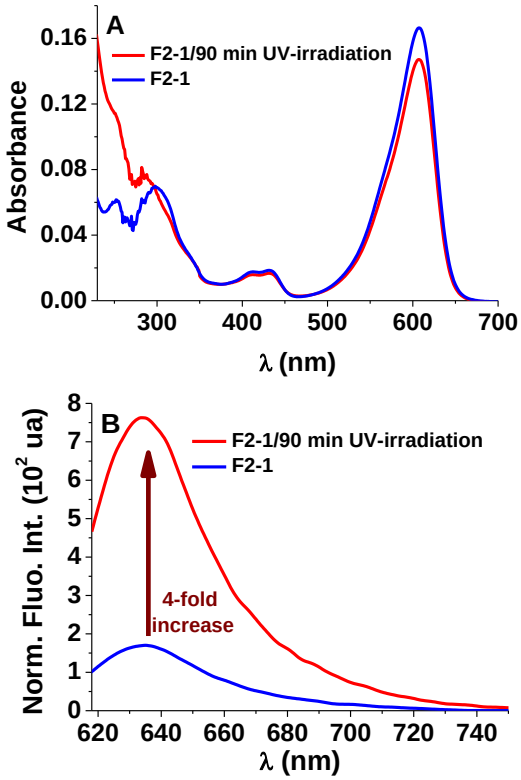

Figure 4. (A) UV-visible absorption spectra and (B) normalized emission (with respect to the absorbance value at the λ_{exc}) spectra of **F2-1** (2.5 µM) at t = 0 and after 90 minutes of UV-photoirradiation at 365 nm in *i*PrOH. λ_{exc} = 618 nm; 1% attenuator; excitation and emission bandwidth = 12.5 nm. The absorption and emission spectra were measured directly after irradiation. The comparison is made by integrating the area under the emission curves. The quantum yield measured for **F2-1** (not irradiated) is 10.6% in *i*PrOH (Figure S28 in the ESI).

These correspond to the first step to the reduction of 1,4-naphthoquinone to 1,4-naphtho-semiquinone ($E^1_{1/2}$ = -0.44 V *vs.* Ag/AgCl/3MKCl) and to the second step to the reduction of the latter to dihydro-1,4-naphthoquinone ($E^2_{1/2}$ = -1.15 V *vs.* Ag/AgCl/KCl(3M)). Each of the redox waves is quasi-reversible, as indicated by the potential difference of about 90 mV between the maxima of the anodic and cathodic peaks. At much more negative potentials, a third 1-electron redox wave ($E^3_{1/2}$ = -1.56 V *vs.* Ag/AgCl/KCl(3M)) of quasi-reversible nature, attributed to the carbonyl of the benzoyl unit, can be observed.[57,58] As anticipated, the redox waves centred on the 1,4-naphthoquinone core are absent for the reduced/protected **10**, and the CV and SWV spectra show the presence of only 2 quasi-reversible redox waves ($E^1_{1/2}$ = -1.44 V and $E^1_{1/2}$ = -1.76 V *vs.* Ag/AgCl/KCl(3M), Figure S37 in the ESI) attributed to the benzoyl carbonyl function. These electrochemical data are consistent with those measured for benzophenone derivatives.[59]

There is scarce electrochemical data available for compounds analogous to the rigid flavylium **8**.[60-63] In DMSO, only an irreversible oxidation peak at 0.32 V (*vs.* Ag/AgCl/KCl(3M)) and an irreversible reduction peak at -0.67 V (*vs.* Ag/AgCl/KCl(3M)) were observed.[62] For these rigid flavylium dyes bearing an amino unit on 4'-position (Scheme 3),[49] a significant intramolecular charge transfer (ICT) is anticipated to take place between the donor (ethylamino substitution) and the acceptor (pyrilium C unit) (Scheme 6-**II**). The irreversible 1-electron reduction might therefore correspond to the reduction of ethanaminium unit to a α-amino radical (Scheme 6-**III**).[64] The latter radical most likely equilibrates with the pyranyl radical (Scheme 6-**IV**). It has been also shown that pyrilium derivatives can undergo an irreversible 1-electron reduction reaction to generate a pyranyl radical, which can rapidly undergo dimerization (Scheme 6-**V**). Such a dimer was shown to undergo a 2-electron oxidation to reinstate the starting pyrilium (Scheme 6).[65,66] The same mechanism was also proposed for some cyanine derivatives.[67] As observed for anilines, the pyrilium stabilized form (Scheme 6-**I**) with an ethylamino substitution can undergo a 1-electron anodic oxidation to lead to an aniline radical cation (Scheme 6-**VI**). The latter can be deprotonated to afford a neutral radical (Scheme 6-**VIII**) or can equilibrate with its resonant structure **VII** (Scheme 6).[68] For **8** whose structure **II** is predominant in solution, we therefore hypothesized an ECE (Electron transfer – Chemical reaction – Electron transfer) mechanism involving structures **I**, **II**, **III**, **IV, VI** and **VII** and explaining the large gap between the reduction and the oxidation peaks. Dimerization observed between two pyranyl radicals or two oxidized aniline radicals (tail-to-tail, head-to-tail or head-to-head coupling) is unlikely to occur due to strong steric interactions that could take place.

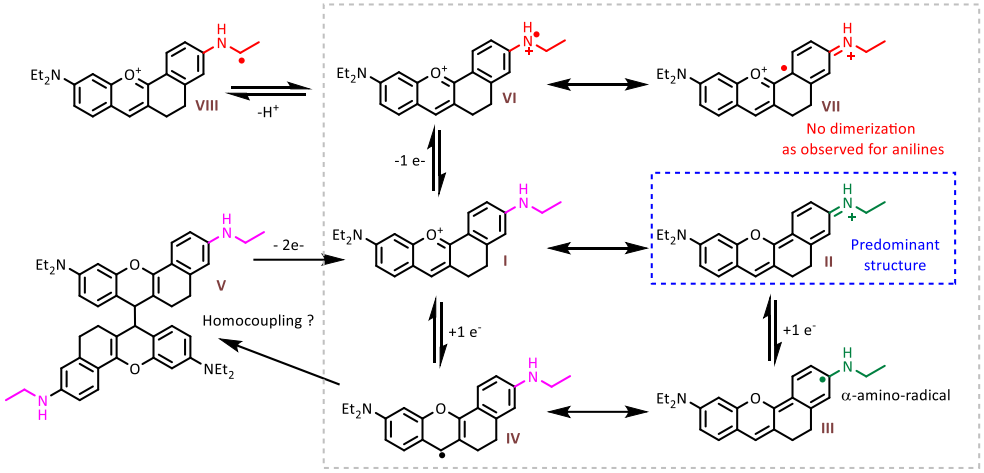

Scheme 6. Putative electrochemical processes occurring with the rigid flavylium prototype dye **8**.

To complement the DFT study and to evaluate the possibility of a PeT process between models **8** and **1**, the oxidation and reduction potentials of the fluorophore **8** in its lowest excited state were evaluated using the Rhem-Weller model (Figures S38-S40 in the ESI) based on the ground state potentials and the absorption spectra recorded in DMSO.[69,70] In the initial stage of the PeT process, a photon is absorbed by **8**, resulting in a photoexcited state with significantly altered redox properties (E^*_{ox} = -1.58 V and E^*_{red} = 1.16 V *vs.* SCE). An electron transfer step thus follows in which the photoexcited state acts as a reductant in the presence of **1** that behaves as an electron acceptor (E^2_{red} = -1.15 V and E^1_{red} = -0.44 V *vs.* SCE). Reduction and protection by methyl groups significantly alters the electrochemical behaviour of the 1,4-naphthoquinone moiety (E^2_{red} = -1.76 V and E^1_{red} = -1.44 V *vs.* SCE), whose electron-donating nature prevents deactivation by PeT.

In the case of the oxidized benzoyl-MDs, CuAAC chemistry with the rigid flavylium dye leads to hybrid assemblies **F1-1** (PEG-1), **F2-1** (PEG-2) and **F3-1** (PEG-3) whose redox properties are significantly modified. Although the redox processes centred on the 1,4-naphthoquinone moiety can be still observed, increasing the PEG chain length has the effect of shifting the redox potentials of the first redox wave towards cathodic potentials (

Table **3** and Figures S37, S41, S43 and S45 in the ESI). The latter is buried under the fluorophore redox peaks, making them difficult to observe. The largest effect is observed for the second redox process centred on the 1,4-naphthoquinone moiety. The shorter the PEG chain, the smaller the potential gap between the two quinone-centred redox waves, increasing gradually from 220 mV for **F1-1** (PEG-1) to 650 mV for **F3-1** (PEG-3) (Figure 5). This suggests that during the 1-electron reduction of the naphthoquinone and flavylium moieties, the resulting radicals are able to associate via radical-radical interactions. These intramolecular interactions thus facilitate the second reduction of the quinone moiety. The longer the PEG chain, the less this type of interaction is favoured, resulting in electrochemical properties centred on the 1,4-quinone unit comparable to those of model **1**.

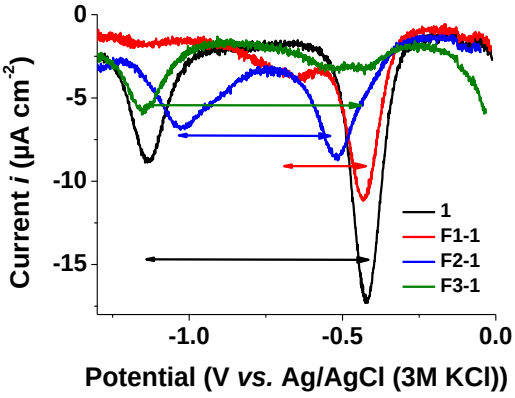

Figure 5. Comparison of the SWV voltamperograms recorded for **1**, **F1-1** (PEG-1), **F2-1** (PEG-2) and **F3-1** (PEG-3). Solvent: DMSO, I = 0.1 M n-Bu_4NPF_6, T = 25°C, v = 200 mV s^{-1}. Reference electrode = Ag/AgCl/KCl(3M), working electrode = glassy carbon disk of 0.07 cm^2 area; auxiliary electrode = Pt wire.

We then turned to the hybrid molecules **F1-10** (PEG-1), **F2-10** (PEG-2) and **F3-10** (PEG-3) in which the benzoyl-MD unit is reduced and protected by methyl groups (Figures S38, S42, S44, S46 and S47 in the ESI). Irrespective of the PEG chain length, the electrochemical behaviour is comparable, demonstrating the absence of redox interactions between the two electrophores. The electrochemical profile of these systems can be defined by the presence of two irreversible redox waves shifted by almost 200 mV (electronic effect of the triazole function) towards cathodic potentials compared to **10** (in some cases the second wave is not observed). For all these systems, a quasi-reversible weak redox wave centred on the flavylium dye can be also observed at potentials comparable to those of **8** (

Table **3**).

Table 3. Redox properties of the hybrid molecules studied by cyclic (CV) and square wave (SVW) voltammetries.

	Benzoyl-MD core									Flavylium core		
	1st redox NQ			2nd redox NQ			3rd redox CO					
Cpd.	E_{pc}	E_{pa}	$E_{1/2}$ CV/SWV	E_{pc}	E_{pa}	$E_{1/2}$ CV/SWV	E_{pc}	E_{pa}	$E_{1/2}$ CV/SWV	E_{pc}	E_{pa}	$E_{1/2}$ CV/SWV
1	-0.49	-0.40	-0.44/-0.42	-1.21	-1.10	-1.15/-1.14	-1.62	-1.50	-1.56/-1.54			
10[a]							-1.49	-1.39	-1.44/-1.41			
							-1.89	-1.64	-1.76/-1.72			
8										-0.67	0.32	nd/-0.62
F1-1	-0.50	-0.42	-0.46/-0.43	-0.73	-0.62	-0.68/-0.65	-1.24	nd	nd/-1.18	nd[b]	nd[b]	nd[b]
F1-10[a]							-1.70	-1.55	-1.63/-1.59	-0.71	-0.59	-0.65/-0.66
							nd	nd	-1.97			
F2-1	-0.55	-0.41	-0.48/-0.52	-1.05	-0.89	-0.97/-1.03	-1.40	nd	nd/-1.29	nd[b]	nd[b]	nd[b]
F2-10[a]							-1.64	-1.53	-1.59/-1.56	-0.78	-0.58	-0.68/-0.65
							-2.07	nd	nd/-1.95			
F3-1	-0.57	-0.47	-0.52/-0.52	-1.21	-1.12	-1.17/-1.15	-1.66	nd	nd/-1.68	nd[b]	nd[b]	nd[b]
F3-10[a]							-1.67	1.56	-1.62/-1.59	nd[b]	-0.30	nd[b]

E_{pc} (potential of the cathodic peak - reduction), E_{pa} (potential of the anodic peak - oxidation), $E_{1/2}$ (half-wave redox potential). E_{pa}, E_{pc} and $E_{1/2}$ are given in V. Solvent: DMSO, I = 0.1 M n-Bu_4NPF_6, T = 25°C, v = 200 mV s^{-1}. Reference electrode = Ag/AgCl/KCl(3M), working electrode = glassy carbon disk of 0.07 cm^2 area; auxiliary electrode = Pt wire. [a] redox processes centred on carbonyl groups. [b] hidden by the 1st benzoyl-MD redox wave. nd = not determined.

Imaging of Model 8 with *P. falciparum* and *P. berghei* Parasitized RBCs

Imaging experiments with *P. falciparum*-pRBCs were then performed with the prototype fluorophore **8**. For this, a culture of mixed developmental stages was incubated for approximately 10 minutes with 500 µM, 50 µM, and 5 µM of **8** prior to imaging (Figure 6). At the highest concentration, we detected staining of the parasite in the DIC image and the fluorescent signal appeared consistent with a nuclear staining (Figure 6A, left). At 50 µM and 5 µM, **8** stained the parasite evenly, with a substantially reduced fluorescent signal in the parasite's food vacuole at the lowest concentration (Figure 6A, middle, right). In addition, at all tested concentrations of **8**, we did neither detect a fluorescent signal of the parasitized host cell nor in uninfected RBCs. We also detected a similar staining pattern with *P. falciparum* sexual stages (gametocytes, Figure 6B) and with asexual stages of the rodent-infecting parasite *P. berghei* when incubated 5 µM **8** (Figure 6C). As short-term exposure to **8** for imaging did not show any adverse effects on the viability of *P. falciparum* 3D7 (chloroquine-sensitive) parasites, we next determined the IC_{50} of **8** (Figure 6D). For this, we cultured the asexual parasites for two developmental cycles in the presence of different concentrations of the fluorophore (two biological replicates in technical triplicates, compared to untreated control = 100 %) and found an IC_{50} of **8** at 0.6 µM. Together, these data suggest that **8** efficiently enters and selectively stains the parasite with no detectable adverse effects over short periods of time.

In vitro Antimalarial Activity

All compounds were then tested for their ability to inhibit the growth of the chloroquine-sensitive *P. falciparum* strain NF54 in culture by determining the concentration of inhibition required to block the growth of the parasite by 50% (IC_{50} values, Table 4). As previously described, 3-benzoyl-MDs, the major metabolites resulting from benzyl oxidation *in vivo*, do not exhibit high antimalarial activity, with IC_{50} values 10-50 times higher than those of the corresponding parent 3-benzyl-MD (e.g. IC_{50}= 2613 ± 557 nM for **PDO** *vs.* IC_{50} = 43 ± 2 nM for **PD**, Table 4) when given externally.[50,71,72] This may be explained by the greater planarity and polarity of 3-benzoyl-MD metabolites compared to their non-oxidised congeners, resulting in very poor internalisation into pRBCs. While this has been very clearly described for **PD** and **PDO**, it remains true after replacement of the CF_3 group by an alkyne function, for the benzyl-MD alkyne **11**[50] (Scheme 3, IC_{50} = 164.2 ± 12, Table 4) and the benzoyl-MD alkyne **1** (IC_{50} = 907 nM, Table 4). The parasite imaging study carried out on **8** showed excellent internalisation of this dye into pRBCs with no apparent adverse effects to these cells over short periods of time. Furthermore, **8** has a low activity in *P. falciparum* (3D7 chloroquine-sensitive strain, Table 4). Compounds substituted by a PEG-azide chain of increasing length (**F1**, **F2** and **F3**, Table 4) were not active in a *P. falciparum* NF54 strain, as shown by IC_{50} values in the µM range in agreement to the first observations with **8** on *P. falciparum* 3D7 strain (IC_{50} about 600 nM). This suggests that the PEG-azido chain has weak to no effect on the antimalarial activity. Interestingly, adducts clicked with an analogue of **PDO** in its oxidised (**F1-1**, **F2-1** and **F3-1**) or reduced/protected (**F1-10**, **F2-10** and **F3-10**) form had IC_{50} values 2 to 3 times lower than benzoyl-MD **1**. This demonstrates that combination with a rigid flavylium cation ensures easier internalisation of the benzoyl-MD derivatives that would be difficult or impossible in the absence of the fluorescent partner. While the click adducts have interesting activities against *P. falciparum*-NF54 strain, the measured IC_{50} values suggest that these hybrid compounds may have potential as fluorogenic redox probes under suitable conditions without altering significantly the pRBCs.

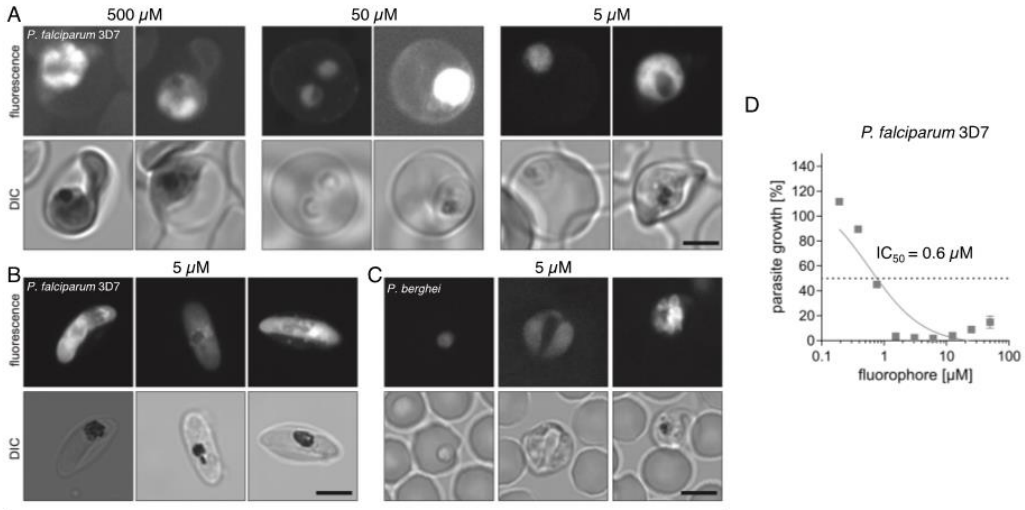

Figure 6. Dye 8 selectively stains *Plasmodium* parasites. **A**) *P. falciparum* infected RBCs of a mixed culture of asexual stages were incubated with **8** at three different concentrations (500 μM, 50 μM, 5 μM) for approximately 10 min and then imaged. **B**) *P. falciparum* gametocytes were incubated with **8** (5 μM) for approximately 10 min and then imaged. **C**) *P. berghei* infected RBCs were incubated with **8** (5 μM) for approximately 10 min and then imaged. Excitation and emission range were as follows: Ex: 561 nm, Em: 570-780 nm, scale bars: 5 μm. **D**) Cytotoxicity assay of synchronized ring stages incubated for two developmental cycles in the presence of different concentrations of **8**. Each concentration was set up in technical triplicates. Parasitemia was assessed by SYBR green intensity. IC_{50} was determined in comparison to untreated control (= 100 %). Mean values of biological duplicates are shown. IC_{50} value was determined using GraphPad Prism with sigmoidal curve fitting (non-linear regression, dose-response inhibition with three-parameters), error bars represent SEM.

Table 4. Averaged IC_{50} values (nM) for 3-benz(o)yl-MD-flavylium adducts and derivatives against *P. falciparum* NF54 strain.[a]

	Cpd.	IC_{50} (nM) *P. falciparum* NF54
Benzyl-MD	**PD**	43 ± 2 (2)[73]
	Alkyne **11**	49 ± 15 (3)[b],[73]
		164.2 ± 12 (3)
Benzoyl-MD	**PDO**	> 1000[72]
		2613 ± 557 (3)
	Alkyne **1**	907 (3)
Flavylium	**8**	600[c]
PEG-1	**F1**	1343 ± 407 (2)
	F1-1	396 ± 74 (2)
	F1-10	241 ± 42 (2)
PEG-2	**F2**	348 ± 107 (2)
	F2-1	314 (1)
	F2-10	331 ± 94 (2)
PEG-3	**F3**	1042 ± 316 (2)
	F3-1	296 ± 80 (2)
	F3-10	318 ± 113 (2)
Controls	Chloroquine	3.9 ± 0.5 (2) ng/ml
	Artesunate	2.1 ± 0.3 (2) ng/ml

[a] Activity against cultured parasites of *P. falciparum* NF54 strain (sensitive to chloroquine) is presented as mean IC_{50} values (the value in brackets indicates the number of replicates). Chloroquine and artesunate were used as standard drugs. [b] IC_{50} value with the SYBR green assay using the *P. falciparum* Dd2 strain assay (resistant strain to chloroquine, sensitive to **PD**, DHA and methylene blue). [c] IC_{50} value with the SYBR green assay using the 3D7 strain (sensitive to chloroquine).-[d] See Scheme 3 for chemical structures.

Conclusion

This work describes, for the first time, the synthesis of rigid flavylium azides and their successful combination, by tethering with variable-length PEG spacers, with drug metabolites (i.e., plasmodione metabolites or benzoyl-MD derivatives) acting as valuable and promising redox cyclers. This approach allowed us to develop, by a screening and selection process, a new series of readily accessible azide fluorescent probes based on rigid flavylium-type dyes, with the ultimate aim of detecting redox changes in pRBCs. By incorporating them by means of CuAAC-type click chemistry to plasmodione analogues in an alkyne form and by optimizing the length of the PEG chain, flavylium/benzoyl-MD hybrid probes with fine-tuned photophysical, electrochemical and biological properties have been prepared and investigated in depth. These probes allow a significant reversible quenching of the fluorescence by a PeT process. The length of the PEG spacer is critical, and the use of a short PEG-1 chain is very likely to induce radical-radical interactions between the reduced species, thereby contributing to the enhancement of the fluorogenic response. With a PEG-3 chain, however, these latter non-covalent interactions are minimized, highlighting only the effects of the PeT process. Taken together, these results emphasize the great potential of these hybrid probes for real-time redox monitoring in parasitized erythrocytes, particularly in conditions where traditional genetically encoded redox probes may fail. As a future perspective, these redox sensors will be used to assess the level of glutathione (thiol redox buffer), one of the endogenous reductants essential for maintaining redox homeostasis in pRBCs. In parallel, the two chromophoric units will be modified to enhance the fluorogenic response of the hybrid probes. The screening approach has indeed revealed substitution patterns that allow the emission spectral window and photoredox properties to be

modified. In addition, the redox properties of diversely substituted benzoyl-MDs have been clearly established. These results pave the way for the study of redox processes in pRBCs, potentially offering a promising toolbox for a better understanding of the mechanisms underlying the action of antimalarial drugs inducing gradients of reactive oxygen species.

Supporting Information

Experimental sections describing antiparasitic activity measurements and cell imaging, dye and hybrid screening (absorption and emission spectra) (Figures S1-S21), physico-chemical properties (Figure S22) photophysical characterization of dyes and hybrids (Tables S1-S2, Figures S23-S36), electrochemical data (Figures S37-S47), dye and hybrid molecules synthesis (Schemes S1-S5) and their characterization by ^{1}H and ^{13}C NMR (Figures S48-S61), DFT calculations (Figures S62-63). The authors have cited additional references within the Supporting Information.[74-82]

Acknowledgements

This work has been published under the framework of the idex Unistra and benefits from a funding (2017/W17RPD29) from the state managed by the French National Research Agency as part of the investments for the future program. The Jean-Marie Lehn Foundation in Strasbourg, France is also acknowledged for funding this work (Post-doc salary to L.C., project Fluoplasmo). The authors also wish to thank the Laboratoire d'Excellence (LabEx) ParaFrap consortium for funding (ANR-11-LABX-0024, E.D.-C.) and creating a proper framework for this scientific research (PhD salary to B.D.) as well as the Agence Nationale de la Recherche, France (Program ANR-PRCI with FNS, Project "ROSaction", grant ANR-22-CE93-0005-01 to E.D-C., M.R., P.M). The authors would like to thank Gilles Ulrich (ICPEES UMR7515 CNRS-Unistra) for making his Fluoromax 4 instrument available for the quantum yield measurements. The authors also warmly thank Manon Aniel, Quentin Riehl, Marc Castelló Escuriet and David García Gallego for partially contributing to this work. D.J. is indebted to the CCIPL/GlidID computational center installed in Nantes for computational resources. M.G. is supported by the Health + Life Science Alliance Heidelberg Mannheim and receives state funding approved by the State Parliament of Baden-Württemberg. This work was further supported by the German Research Foundation – project number 240245660 – SFB 1129 to MG. The authors are grateful to the Infectious Diseases Imaging Platform (IDIP) at the Center for Infectious Diseases, Heidelberg, Germany, for the microscopy support. This research used resources of the GLiCID Computing Facility (Ligerien Group for Intensive Distributed Computing, https://doi.org/10.60487/glicid, Pays de la Loire, France).

Keywords: Click chemistry • fluorophore azide • redox probe • flavylium • PeT process

[1] A. K. Aranda-Rivera, A. Cruz-Gregorio, Y. L. Arancibia-Hernández, E. Y. Hernández-Cruz, J. Pedraza-Chaverri, *Oxygen* **2022**, *2*, 437.

[2] I. Liguori, G. Russo, F. Curcio, G. Bulli, L. Aran, D. Della-Morte, G. Gargiulo, G. Testa, F. Cacciatore, D. Bonaduce, P. Abete, *CIA* **2018**, *13*, 757.

[3] L. Wu, A. C. Sedgwick, X. Sun, S. D. Bull, X.-P. He, T. D. James, *Acc. Chem. Res.* **2019**, *52*, 2582.

[4] L. Zhang, L. Zhang, X. Zhang, Y. Zhao, S. Fang, J. You, L. Chen, *TrAC, Trends Anal. Chem.* **2023**, *169*, 117377.

[5] G. G. Martinovich, S. N.Cherenkevich, H. Sauer, *Eur. Biophys. J.* **2005**, *34*, 937.

[6] Y. Sun, P. Sun, W. Guo, *Coord. Chem. Rev.* **2021**, *429*, 213645.

[7] X. Jiang, L. Wang, S. L. Carroll, J. Chen, M. C. Wang, J. Wang, *Antioxid. Redox Signal.* **2018**, *29*, 518.

[8] F. Mohring, E. Jortzik, K. Becker, *Mol. Biochem. Parasitol.* **2016**, *206*, 75.

[9] F. Mohring, M. Rahbari, B. Zechmann, S. Rahlfs, J. M. Przyborski, A. J. Meyer, K. Becker, *Free Rad. Biol. Med.* **2017**, *104*, 104.

[10] A. I. Kostyuk, A. S. Panova, D. S. Bilan, V. V. Belousov, *Free Rad. Biol. Med.* **2018**, *128*, 23.

[11] D. Kasozi, F. Mohring, S. Rahlfs, A. J. Meyer, K. Becker, *PLoS Pathog.* **2013**, *9*, e1003782.

[12] K. C. Heimsch, C. G. W. Gertzen, A. K. Schuh, T. Nietzel, S. Rahlfs, J. M. Przyborski, H.Gohlke, M. Schwarzländer, K. Becker, K. Fritz-Wolf, *Antioxid. Redox Signal.* **2022**, *37*, 1.

[13] A. J. Meyer, T. P. Dick, *Antioxid. Redox Signal.* **2010**, *13*, 621.

[14] N. Andreu, A. Zelmer, S. Wiles, *FEMS Microbiol. Rev.* **2011**, *35*, 360.

[15] X. Bai, K. K.-H. Ng, J. J. Hu, S. Ye, D. Yang, *Annu. Rev. Biochem.* **2019**, *88*, 605.

[16] A. Weidinger, A. Kozlov, *Biomolecules* **2015**, *5*, 472.

[17] X. Jiang, L. Wang, S. L. Carroll, J. Chen, M. C. Wang, J. Wang, *Antioxid. Redox Signal.* **2018**, *29*, 518.

[18] L. Zhang, L. Zhang, X. Zhang, Y. Zhao, S. Fang, J. You, L. Chen, *TrAC, Trends Anal. Chem.* **2023**, *169*, 117377.

[19] A. Kaur, E. J. New, *Acc. Chem. Res.* **2019**, *52*, 623.

[20] S. Y. Park, S. A. Yoon, Y. Cha, M. H. Lee, *Coord. Chem. Rev.* **2021**, *428*, 213613.

[21] X. Jiao, Y. Li, J. Niu, X. Xie, X. Wang, B. Tang, *Anal. Chem.* **2018**, *90*, 533.

[22] X. Chen, X. Tian, I. Shin, J. Yoon, *Chem. Soc. Rev.* **2011**, *40*, 4783.

[23] Z. Wu, Y. Guo, W. Jiang, Y. Yang, P. Wei, T. Yi, *TrAC, Trends Anal. Chem.* **2024**, *170*, 117461.

[24] Y. Huang, X. Cao, Y. Deng, X. Ji, W. Sun, S. Xia, S. Wan, H. Zhang, R. Xing, J. Ding, C. Ren, *Talanta* **2024**, *268*, 125275.

[25] A. Kaur, J. L. Kolanowski, E. J. New, *Angew. Chem. Int. Ed.* **2016**, *55*, 1602.

[26] B. Li, Z. He, H. Zhou, H. Zhang, T. Cheng, *Chin. Chem. Lett.* **2017**, *28*, 1929.

[27] Z. Lou, P. Li, K. Han, *Acc. Chem. Res.* **2015**, *48*, 1358.

[28] J. Zhan, W. Song, E. Ge, L. Dai, W. Lin, *Coord. Chem. Rev.* **2023**, *493*, 215321.

[29] N. Kwon, D. Kim, K. M. K. Swamy, J. Yoon, *Coord. Chem. Rev.* **2021**, *427*, 213581.

[30] G. G. Dias, A. King, F. De Moliner, M. Vendrell, E. N. Da Silva Júnior, *Chem. Soc. Rev.* **2018**, *47*, 12–27.

[31] S. T. Manjare, Y. Kim, D. G. Churchill, *Acc. Chem. Res.* **2014**, *47*, 2985.

[32] L. Tian, H. Feng, Z. Dai, R. Zhang, *J. Mater. Chem. B* **2021**, *9*, 53.

[33] B. Kalyanaraman, M. Hardy, R. Podsiadly, G. Cheng, J. Zielonka, *Arch. Biochem. Biophys.* **2017**, *617*, 38.

[34] L. Jeuken,; M. Orrit,; G. Canters, *Curr. Opin. Electrochem.* **2023**, *37*, 101196.

[35] V. Goulle, A. Harriman, J.-M. Lehn, *J. Chem. Soc., Chem. Commun.* **1993**, 1034.

[36] Y.-X. Yuan, Y. Chen, Y.-C. Wang, C.-Y. Su, S.-M. Liang, H. Chao, L.-N. Ji, *Inorg. Chem. Commun.* **2008**, *11*, 1048.

[37] A. C. Benniston, G. Copley, K. J. Elliott, R. W. Harrington, W. Clegg, *Eur J. Org. Chem.* **2008**, *2008*, 2705.

[38] L. E. Greene, R. Godin, G. Cosa, *J. Am. Chem. Soc.* **2016**, *138*, 11327.

[39] L. Han, M. Liu, D. Ye, N. Zhang, E. Lim, J. Lu, C. Jiang. *Biomater.***2014**, *35*, 2952.

[40] I. Heing-Becker, K. Achazi, R. Haag, K. Licha, *Dyes Pigm.* **2022**, *201*, 110198.

[41] J. Zheng, Q. Zeng, R. Zhang, D. Xing, T. Zhang, *J. Am. Chem. Soc.* **2019**, *141*, 19226.

[42] D. P. Kennedy, C. M. Kormos, S. C. Burdette, *J. Am. Chem. Soc.* **2009**, *131*, 8578.

[43] F. Yu, P. Li, P. Song, B. Wang, J. Zhao, K. Han, *Chem. Commun.* **2012**, *48*, 4980.

[44] R. M. Kierat, B. M. B. Thaler, R. Krämer. *Bioorg. Med. Chem. Lett.* **2010**, *20*, 1457.

[45] W. Zhang, P. Li, F. Yang, X. Hu, C. Sun, W. Zhang, D. Chen, B. Tang, *J. Am. Chem. Soc.* **2013**, *135*, 14956.

[46] W. Zhang, X. Wang, P. Li, F. Huang, H. Wang, W. Zhang, B. Tang, *Chem. Commun.* **2015**, *51*, 9710.

[47] T.-L. Shie, C.-H. Lin, S.-L. Lin, D.-Y. Yang, *Eur. J. Org. Chem.* **2007**, 4831.

[48] R. A. Illos, D. Shamir, L. J. W. Shimon, I. Zilbermann, S. Bittner, *Tet. Lett.* **2006**, *47*, 5543.

[49] B. Dupouy, A. Hemmerlin, Q. Chevalier, V. Mazan, H. Schaller, E. Davioud-Charvet, M. Elhabiri, To be submitted **2024**.

[50] B. A. Cichocki, V. Khobragade, M. Donzel, L. Cotos, S. Blandin, C. Schaeffer-Reiss, S. Cianférani, J.-M. Strub, M. Elhabiri, E. Davioud-Charvet, *JACS Au* **2021**, *1*, 669.

[51] I. Iacobucci, V. Monaco, A. Hovasse, B. Dupouy, R. Keumoe, B. Cichocki, M. Elhabiri, B. Meunier, J. M. Strub, M. Monti, S. Cianférani, S. A. Blandin, C. Schaeffer-Reiss, E. Davioud-Charvet, *ChemBioChem* **2024**, *25*, e202400187.

[52] H. Görner, *J. Photochem. Photobiol. A: Chem.* **2004**, *165*, 215.

[53] J. R. Poulsen, J. W. Birks, *Anal. Chem.* **1989**, *61*, 2267.

[54] N. Trometer, B. Cichocki, Q. Chevalier, J. Pécourneau, J.-M. Strub, A. Hemmerlin, A. Specht, E. Davioud-Charvet, M. Elhabiri, *J. Org. Chem.* **2024**, *89*, 2104.

[55] M. Donzel, M. Elhabiri, E. Davioud-Charvet, *J. Org. Chem.* **2021**, *86*, 10055.

[56] H. Görner, *Photochem Photobiol Sci* **2004**, *3*, 71.

[57] P. Sidorov, I. Desta, M. Chessé, D. Horvath, G. Marcou, A. Varnek, E. Davioud-Charvet, M. Elhabiri, *ChemMedChem* **2016**, *11*, 1339.

[58] L. Cotos, M. Donzel, M. Elhabiri, E. Davioud-Charvet, *Chem. Eur. J.* **2020**, *26*, 3314

[59] R. F. Michielli, P. J. Elving, *J. Am. Chem. Soc.* **1968**, *90*, 1989.

[60] E. C. Prima, A. Nuruddin, B. Yuliarto, G. Kawamura, A. Matsuda, *New J. Chem.* **2018**, *42*, 11616.

[61] J. Avó, V. Petrov, N. Basílio, A. Jorge Parola, F. Pina, *Dyes Pigm.***2016**, *135*, 86.

[62] P. Ferreira Da Silva, J. C. Lima, F. H. Quina, A. L. Maçanita, *J. Phys. Chem. A* **2004**, *108*, 10133.

[63] A. L. Pinto, P.Máximo, J. Pina, G. Calogero, C. A. T. Laia, A. J. Parola, J. C. Lima, *Dyes Pigm.* **2023**, *218*, 111495.

[64] J. A. Leitch, T. Rossolini, T. Rogova, J. A. P. Maitland, D. J. Dixon, *ACS Catal.* **2020**, *10*, 2009.

[65] N. T. Berberova, G. N. Dorofeenko, O. Y. Okhlobystin, *Chem. Heterocycl. Compd.* **1977**, *13*, 250.

[66] B. Guel, D. Tountian, Y. Bonzy-Coulibaly, H. Traore, F. Sié Sib, *C. R. Chimie* **2007**, *10*, 535.

[67] J. R. Lenhard, A. D. Cameron, *J. Phys. Chem.* **1993**, *97*, 4916.

[68] J. S. Jaworski, M. K. Kalinowski In *PATAI'S Chemistry of Functional Groups*, (Ed. Z. Rappoport), Wiley, **2007**; p 871.

[69] L. Buzzetti, G. E. M. Crisenza, P. Melchiorre, *Angew. Chem. Int. Ed.* **2019**, *58*, 3730.

[70] P. Suppan, E. Vauthey, *J. Photochem. Photobiol. A: Chem.* **1989**, *49*, 239.

[71] L. Feng, D. A. Lanfranchi, L. Cotos, E. Cesar-Rodo, K. Ehrhardt, A.-A. Goetz, H. Zimmermann, F. Fenaille, S. A. Blandin, E. Davioud-Charvet, *Org. Biomol. Chem.* **2018**, *16*, 2647.

[72] T. Müller, L. Johann, B. Jannack, M. Brückner, D. A. Lanfranchi, H. Bauer, C. Sanchez, V. Yardley, C. Deregnaucourt, J. Schrével, M. Lanzer, R. H. Schirmer, E. Davioud-Charvet, *J. Am. Chem. Soc.* **2011**, *133*, 11557.

[73] B. Dupouy, M. Donzel, M. Roignant, S. Charital, R. Keumoe, Y. Yamaryo-Botté, A. Feckler, M. Bundschuh, Y. Bordat, M. Rottmann, P. Mäser, C. Y. Botté, S. A. Blandin, S. Besteiro, E. Davioud-Charvet, *ACS Inf. Dis.* **2024**, *10*, 3553.

Entry for the Table of Contents

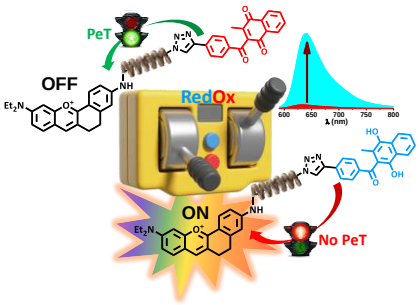

Redox-sensitive pro-fluorophores based on azido-flavyliums clicked to alkynyl analogues of plasmodione oxide have been developed. In their quinone form, the fluorescence is quenched by photoinduced electron process (PeT) and restored after reducing to hydroquinone. PEG chain length modulates the amplitude of fluorogenic response. Due to their properties, these hybrid compounds have the potential to evaluate redox alterations in parasitized erythrocytes.

Institute and/or researcher Twitter usernames: @redoxLCBM, @LIMA_UMR7042, @ecpm_Unistra, @INC_CNRS, @unistra, @UHA68, @ParaFrap